

Application of extended Kalman filter for estimation of periodic disturbance and velocity ripple reduction in PMSM drive

Ł.J. NIEWIARA^{1*}, T. TARCZEWSKI¹, and L.M. GRZESIAK²

¹Department of Automatics and Measurement Systems, Nicolaus Copernicus University in Torun, ul. Grudziadzka 5, 87-100 Torun, Poland

²Institute of Control and Industrial Electronics, Warsaw University of Technology, ul. Koszykowa 75, 00-662 Warsaw, Poland

Abstract. In this paper an application of extended Kalman filter (EKF) for estimation and attenuation of periodic disturbance in permanent magnet synchronous motor (PMSM) drive is investigated. Most types of disturbances present into PMSM drive were discussed and described. The mathematical model of the plant is presented. Detailed information about the design process of the disturbance estimator was introduced. A state feedback controller (SFC) with feedforward realizes the regulation and disturbance compensation. The theoretical analysis was supported by experimental tests on the laboratory stand. Both time- and frequency-domain analysis of the estimation results and angular velocity were performed. A significant reduction of velocity ripple has been achieved.

Key words: extended Kalman filter, disturbance estimation, PMSM drive, pulsating torque, velocity ripple reduction.

1. Introduction

Modern motion control systems utilize more and more frequent drive systems with alternating current (AC) machines [1]. In recent years permanent magnet synchronous motors (PMSMs) became special interest caused by their superior features, i.e. high power density and efficiency, low noise, free maintenance and a favorable torque-to-inertia ratio [1–4]. As a consequence of above mentioned advantages, PMSMs find a wide range of industrial applications, including robotics, aerospace, machine tools, engines for electric vehicles and power generation [1–3, 5].

Regardless of all of the listed advantages of drive systems with PMSMs, precise and high-quality control is still not a trivial issue. In general, the main drawback is caused by the undesired disturbances, manufacturing imperfections and uncertainties, which deteriorate the operating quality of the drive, introducing pulsating torque and in effect angular velocity ripple [1, 2]. Commonly, the drive system is fed from pulse-width modulated power inverters, which also impacts negatively the produced electromagnetic torque. In this case the main issue lies in current measurements errors and switching devices. The aforementioned effects deteriorate the stator currents and voltages, which introduces additional disturbances into control system and distorts the electromagnetic torque produced by the machine [4, 6]. In such a case, one of the possible solutions, able to overcome the undesired phenomena, is to employ advanced control algorithms [1, 2]. In the last decades, numerous control algorithms were developed in order to achieve high operation quality and enhanced control per-

formance. A lot of control techniques dedicated for AC machine drives can be found in the literature, for example model predictive control (MPC) [7, 8], internal model control (IMC) [9], proportional-integral-derivative (PID) controllers with disturbance compensation [10–12], active disturbance rejection control (ADRC) [6, 13, 14], disturbance observer-based control (DOBC) [2, 15–18], artificial neural networks based control (ANNC) [19, 20] and state feedback control (SFC) [2, 21, 22], to name a few.

In the last few decades, it has been recognized that a relevant task for controller design for PMSM drives is to ensure compensation of a wide range of external disturbances and to improve robustness for the uncertainties present in the drive system in order to guarantee highest possible quality of operation. Therefore, the first focus of this paper is to perform comprehensive analysis of the most common kinds of disturbances/uncertainties in typical PMSM, related to the construction of the machine and the inverter (i.e. measurement accuracy and dead-time effect). It should be noted that the disturbance/uncertainty estimation and attenuation (DUEA) techniques seem to be one of the most promising control strategies in the recent years [1]. Those control methods are based on the same fundamental idea for disturbance/uncertainties estimator employment. The estimate is introduced into a compensation mechanism, which allows to improve the operation quality of the drive. In such a case, the introduction of complex disturbance models into control system is not necessary [1]. The above mentioned ADRC and DOBC belong to the category of DUEA. The implementation of a DOBC based control algorithm forces the employment of an observer, which is capable for proper reconstruction of the disturbance present in a drive. This is a crucial issue determining the effectiveness of the designed control system. Therefore, the main focus of this paper is to investigate the estimation properties and disturbance attenuation of the proposed algorithm. The reconstructed disturbance

*e-mail: lukniewiara@umk.pl

Manuscript submitted 2020-01-09, revised 2020-04-06, initially accepted for publication 2020-04-11, published in October 2020

signal is introduced into control structure for angular velocity ripple reduction. A state feedback controller with feedforward path was employed and investigated.

The earlier depicted effects are related to both the electric and mechanical angle [23–25]. Therefore, the basic-frequency of the periodic disturbances depends on the angular velocity of the motor shaft. It means, that the frequency of the harmonics is varying with the given rotational speed. Therefore, the pulsating torque has a significant effect mainly at low-speeds [2, 11]. The mechanical part of the machine is a kind of low-pass filter and it reduces the impact of higher order harmonics. The problem appears for low-frequency harmonics, which cannot be rejected by the inertia or by the bandwidth of the speed control loop [11]. In such circumstances, the improvement of drive operation quality should be realized mainly for low-speeds. It has been proven in [2, 6, 10] that introduction of disturbance estimator into the control system successfully reduces the angular velocity ripple for low angular velocities of the motor. This indicates that the most critical issue is a proper estimation of disturbances in above mentioned operating region. Taking this into account, the investigations presented in this paper were realized for rotational speeds in the range of 1–5% of the rated value.

In this paper, an extended Kalman filter (EKF) is investigated in application for estimation of periodic disturbance present in a PMSM drive. A detailed analysis of the nature of the undesired phenomena is taken into account. A discrete plant model was determined and applied into estimation algorithm. Experimental tests were carried out on a laboratory stand equipped with a drive system based on 2-level voltage source inverter (VSI) with PMSM. For selected operating points, detailed time- and frequency-domain analyses were conducted. Obtained results were confronted with the theoretical expectations. The estimated disturbance signal is employed for reduction of angular velocity ripple of the drive. This task is realized using a SFC with feedforward path. The initial investigations of the proposed estimation algorithm were presented in [26]. The performed analysis indicates that an EKF may be successfully applied for reconstruction of periodic disturbances present in a drive system with PMSM. This paper is an extended version of the basic concept, investigating the ability of disturbances attenuation of a SFC with feedforward path enhanced by EKF. To the best Authors' knowledge, there are no other works investigating in detail the estimation results of employed load torque observer for periodic disturbances present in a PMSM drive.

The rest of this paper is organized as follows. Section 2 contains an overview of sources of periodic disturbances in PMSM drive. Section 3 describes the mathematical model of the plant in the rotating reference dq -frame. Section 4 discusses the design process of proposed estimation algorithm based on EKF, introducing a discrete-time domain model. In Section 5, the detailed information about developed disturbance estimator is presented. Section 6 describes the employed control structure based on a state feedback controller. Section 7 demonstrates results of experimental tests and contains a detailed analysis in time- and frequency-domain. Finally, Section 8 concludes the paper.

2. Periodic disturbance present in PMSM drive

The assessment of estimation quality requires the knowledge about the nature of disturbances and uncertainties present in the investigated drive system. From this point of view, it is very important to understand and identify the complex nature of the mentioned phenomena. The sources of undesired disturbances and uncertainties may be assigned in following groups [1, 6, 10, 15, 23]: inverter caused, machine design and manufacturing tolerances related. In general, the first group is responsible for production of torque ripple [15], while the other two produce cogging torque and are responsible for flux harmonics [1, 15, 23]. The general distribution of torque ripple sources is presented in Fig. 1.

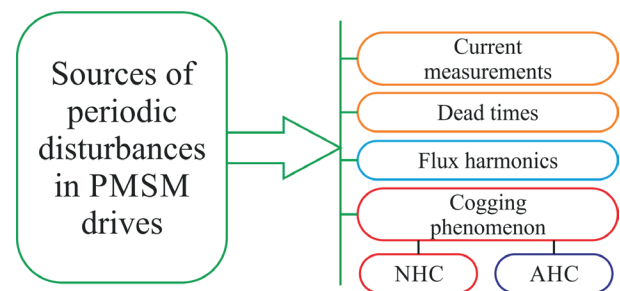


Fig. 1. Sources of periodic disturbances in PMSM drives

Due to errors of phase currents measurements and dead-time effects present in inverter based drive systems, either the stator voltages and currents are distorted, causing periodic disturbances related to the first, second and sixth harmonic of the basic-component of stator currents [1, 6]. The offset- and scaling-errors impact directly the phase currents, causing ripple in the rotating dq frame, which can be modelled as follows [1, 6, 11]:

$$d_{dC}^{\text{off}} = d^{\text{off}} \sin(p\theta_m + \alpha_{\text{off}}), \quad (1)$$

$$d_{qC}^{\text{off}} = d^{\text{off}} \cos(p\theta_m + \alpha_{\text{off}}), \quad (2)$$

$$d_{dC}^{\text{scl}} = d^{\text{scl}} \sin(2p\theta_m + \alpha_{\text{scl}}), \quad (3)$$

$$d_{qC}^{\text{scl}} = d^{\text{scl}} \cos(2p\theta_m + \alpha_{\text{scl}}), \quad (4)$$

where: d_{dC}^{off} , d_{qC}^{off} , d_{dC}^{scl} , d_{qC}^{scl} – errors of current offset and scaling in d - and q -axis, respectively, d^{off} , d^{scl} – amplitude of offset- and scaling-error, θ_m – mechanical angle, α_{off} , α_{scl} – angular displacement of offset and scaling error, respectively, p – number of pole pairs. It should be noted, that the relation between the electrical angle θ_e and mechanical angle θ_m is given by: $\theta_e = p\theta_m$.

The dead-times cause a loss of a portion of duty cycle and therefore deteriorate the voltage applied to the stator [1, 6, 24]. This effect may be represented on the phase current channels in the d - q reference frame as follows [24]:

$$d_{dC}^{d-t} = \sum_{i=1}^{+\infty} d_{di} \sin(6ip\theta_m), \quad (5)$$

$$d_{qC}^{d-t} = \sum_{i=1}^{+\infty} d_{qi} \cos(6ip\theta_m). \quad (6)$$

where: d_{dC}^{d-t} , d_{qC}^{d-t} – sixth order harmonics in $d-q$ frame, d_{di} , d_{qi} – amplitude of sixth harmonic, i – the order of harmonic.

The above depicted phenomena deteriorates the produced electromagnetic torque. Assuming a zero d -axis current and equal values of the direct and quadrature components of the inductance, the produced electromagnetic torque of the motor is given by [1, 6]:

$$d_T^{\text{inv}} = \frac{3}{2} p \Psi_f \Delta i_q \quad (7)$$

with:

$$\Delta i_q = d_{qC}^{\text{off}} + d_{qC}^{\text{scl}} + d_{qC}^{d-t},$$

where: d_T^{inv} – periodic disturbance caused by the inverter.

Since the neodymium-iron-boron is the most widely used material for the production of permanent magnets (PMs), flux density is easily affected by the temperature variation. The impact of flux variations on produced torque can be defined in the following form [1, 11]:

$$d_i^{\text{flux}} = \frac{3}{2} p i_q \sum_{i=1}^{+\infty} \Psi_{fi} \cos(6i\theta_e) = \frac{3}{2} p i_q \sum_{i=1}^{+\infty} \Psi_{fi} \cos(6ip\theta_m), \quad (8)$$

where: Ψ_{fi} – denotes the magnitude of the sixth order harmonic and its multiples given by the subscript i .

The cogging torque is mainly caused by the presence of stator slots, which cause the changes of magnetic reluctance during rotor movement. It is composed of several harmonic components which can be classified into two groups [23, 25]. The first group is an array of native harmonic components (NHC) which originate in the combination of design parameters, i.e. number of stator slots n_S and pole-pairs p . The second group is an array of additional harmonic components (AHC) which are the consequence of material and assembly imperfections, which are directly related to number of stator slots n_S and number of poles n_P ($n_P = 2p$). They are not present in a perfectly manufactured motor. In general, this undesired torque component can be expressed as [23, 25, 27]:

$$d_T^{\text{cog}} = d_{NHC}^{\text{cog}} + d_{AHC}^{\text{cog}} \quad (9)$$

with:

$$d_{NHC}^{\text{cog}} = \sum_{i=1}^{+\infty} d_{NHCi} \sin(LCM(n_S, n_P) i \theta_m + \gamma_{NHCi})$$

$$d_{AHC}^{\text{cog}} = \sum_{i=1}^{+\infty} d_{AHCi}^R \sin(n_S i \theta_m + \gamma_{AHCi}^R) + \sum_{i=1}^{+\infty} d_{AHCi}^S \sin(n_P i \theta_m + \gamma_{AHCi}^S),$$

where: $LCM(n_S, n_P)$ – the least common multiple between the number of slots and poles, d_{NHC}^{cog} , d_{AHC}^{cog} – native and additional

component of the cogging torque, respectively, d_{NHCi} , d_{AHCi}^R , d_{AHCi}^S – amplitude of i th-order native and additional (R – rotor, S – stator) harmonic component, respectively, γ_{NHCi} , γ_{AHCi}^R , γ_{AHCi}^S – angular displacement of i th-order native and additional (R – rotor, S – stator) harmonic components of cogging torque, respectively.

The above presented disturbance components influence the drive system affecting its operating quality, increasing the amplitude of velocity ripple, vibrations and acoustic noise [2]. A well-designed disturbance observer should be able to estimate all harmonic components present in the drive system. This is a non-trivial issue since the plant model is non-linear. Therefore, an extended Kalman filter algorithm was adopted for disturbance estimation.

3. Mathematical model of the drive system

The design process of state observer should be based on the mathematical model of the system. Since the estimation algorithm is implemented in a microcontroller based device, the plant model should be described in discrete-time domain. In such a case it is necessary to transform the continuous time based model into the discrete-time domain. The considered drive system with PMSM is described by following continuous time equations in a rotating reference frame [1, 2, 18, 28]:

$$L_d \frac{di_d(t)}{dt} = u_d(t) - R_s i_d(t) + p \omega_m(t) L_q i_q(t), \quad (10)$$

$$L_q \frac{di_q(t)}{dt} = u_q(t) - R_s i_q(t) - p \omega_m(t) [L_d i_d(t) + \Psi_f], \quad (11)$$

$$J_m \frac{d\omega_m(t)}{dt} = \left[\frac{3}{2} p \Psi_f + (L_d - L_q) i_d(t) \right] i_q(t) - T_o(t), \quad (12)$$

where: $i_d(t)$, $i_q(t)$, $u_d(t)$, $u_q(t)$ – space vector components of stator currents and voltages in d - and q -axis, respectively, R_s – stator resistance, L_d , L_q – stator inductance components, p – number of pole pairs, Ψ_f – magnet flux linkage, $\omega_m(t)$ – angular velocity of the rotor, J_m – moment of inertia, $T_o(t)$ – overall load torque. Since the considered motor is a surface mounted machine, the inductance components are equal, i.e. $L_d = L_q = L_s$.

It is worth pointing out that in (12) considered overall load torque $T_o(t)$ is a sum of the periodic disturbance present in the drive system, friction torque and external load torque. It may be described using the following formula:

$$T_o(t) = T_{\text{per}}(t) + T_b(t) + T_l(t), \quad (13)$$

$T_b(t)$ – viscous friction torque, it is approximately constant for a steady-state and proportional to the angular velocity, $T_l(t)$ – external load torque, this component is related to the load torque applied to the motor shaft. A well-designed estimator should be able to estimate all components given by (13). This task may be realized using an extended Kalman filter algorithm. It should be noted that the periodic disturbance present in the drive system

is a resultant of the components defined by equations (7)–(9) and is given as follows [1]:

$$T_{\text{per}}(t) = d_T^{\text{inv}} + d_T^{\text{flux}} + d_T^{\text{cog}}, \quad (14)$$

where the following components d_T are caused by the inverter (*inv*), flux harmonics (*flux*) and the native and additional components of cogging effect (*cog*).

4. Design process of disturbance estimator

The EKF based estimators are mainly employed for angular position or velocity estimation in sensorless control [28–30]. In such a case the defined model is described in stationary $\alpha\beta$ -frame [29, 30] or combined $\alpha\beta/dq$ -frame [28]. This causes relatively high computational effort, due to complex non-linear character of the assumed description. The computational effort may be decreased, for example, using a reduced order observer [30]. Since the developed estimator is employed mainly for disturbance reconstruction, the assumed full-order mathematical model of the plant can be defined in the rotating reference dq frame [31]. In such a case the input and output matrices in the overall mathematical description of the plant become stationary, reducing the computational complexity of the developed disturbance estimator. It should be noted that the introduction of a full order mathematical model of the plant given in dq -frame makes it possible to estimate the periodic component of the disturbance in respect to (7)–(9).

First of all, the continuous mathematical model given by (10)–(12) should be transformed into discrete-time domain. In such a case, a backward-Euler approximation method may be employed. It should be noted that in order to ensure convergence between the discrete and continuous model, the sampling time should be properly selected in respect to the electrical and mechanical time-constant [32, 33]. The derivative can be rewritten using the following equation [33]:

$$\frac{dx_n(t)}{dt} = \frac{x_{n_k} - x_{n_{k-1}}}{T_s}, \quad (15)$$

where: x_n – state variable, k – discrete time domain index, T_s – discrete sampling time.

Taking into account (15) in (10)–(12) following formulas will be obtained [31]:

$$i_{d_k} = \left(1 - \frac{T_s}{L_s} R_s\right) i_{d_{k-1}} + pT_s \omega_{m_{k-1}} i_{q_{k-1}} + \frac{T_s}{L_s} u_{d_{k-1}}, \quad (16)$$

$$i_{q_k} = \left(1 - \frac{T_s}{L_s} R_s\right) i_{q_{k-1}} - pT_s \omega_{m_{k-1}} \left[i_{d_{k-1}} + \frac{\Psi_f}{L_s} \right] + \frac{T_s}{L_s} u_{q_{k-1}}, \quad (17)$$

$$\omega_{m_k} = K_t \frac{T_s}{J_m} i_{q_{k-1}} + \omega_{m_{k-1}} - \frac{T_s}{J_m} T_{o_{k-1}}, \quad (18)$$

where: $K_t = \frac{3}{2} p \Psi_f$ – torque constant.

The equations (16)–(18) describe the state variables of the mathematical model of the drive system in discrete-time domain. The state-space vector of the drive system was chosen on the basis of the defined discrete model [2, 31]:

$$\mathbf{x}_k = [i_{d_k} \ i_{q_k} \ \omega_{m_k} \ T_{o_k}]^T, \quad (19)$$

where: \mathbf{x}_k – vector of state-variables in discrete time domain.

The overall load torque $T_o(t)$ is treated as a state variable, therefore some assumptions should be made before, i.e. the estimated signal is similar to white noise and it is constant for a single sampling period [28, 31]:

$$\frac{dT_o(t)}{dt} \approx 0 \rightarrow T_{o_k} \cong T_{o_{k-1}}. \quad (20)$$

Taking into account (16)–(20) the overall discrete mathematical model of the system may be described in the following form:

$$\mathbf{x}_k = \mathbf{f}(\mathbf{x}_{k-1}, \mathbf{u}_{k-1}, k) + \mathbf{w}_k = \mathbf{A}_{d_{k-1}} \mathbf{x}_{k-1} + \mathbf{B}_d \mathbf{u}_{k-1} + \mathbf{w}_k, \quad (21)$$

$$\mathbf{y}_k = \mathbf{h}(\mathbf{x}_k, k) + \mathbf{v}_k = \mathbf{C} \mathbf{x}_k + \mathbf{v}_k \quad (22)$$

with:

$$\mathbf{A}_{d_{k-1}} = \begin{bmatrix} 1 - \frac{T_s}{L_s} R_s & pT_s \omega_{m_{k-1}} & 0 & 0 \\ -pT_s \omega_{m_{k-1}} & 1 - \frac{T_s}{L_s} R_s & -pT_s \frac{\Psi_f}{L_s} & 0 \\ 0 & K_t \frac{T_s}{J_m} & 1 & -\frac{T_s}{J_m} \\ 0 & 0 & 0 & 1 \end{bmatrix},$$

$$\mathbf{B}_d = \begin{bmatrix} \frac{T_s}{L_s} & 0 \\ 0 & \frac{T_s}{L_s} \\ 0 & 0 \\ 0 & 0 \end{bmatrix}, \quad \mathbf{u}_{k-1} = \begin{bmatrix} u_{d_{k-1}} \\ u_{q_{k-1}} \end{bmatrix},$$

$$\mathbf{C} = \begin{bmatrix} 1 & 0 & 0 & 0 \\ 0 & 1 & 0 & 0 \\ 0 & 0 & 1 & 0 \end{bmatrix},$$

where: $\mathbf{A}_{d_{k-1}}$ – non-stationary state matrix (discrete-time domain), \mathbf{B}_d – input matrix (discrete-time domain), \mathbf{u}_{k-1} – input vector of the system (discrete-time domain), \mathbf{C} – output matrix, \mathbf{y}_k – output of the system (discrete-time domain), \mathbf{w}_k – process noise, \mathbf{v}_k – measurement noise.

The assumed discrete mathematical model of the system is given in the rotating reference frame. It has been assumed that all of the state variables of the motor, i.e. currents (i_d , i_q) and angular velocity (ω_m), are measured. The overall load torque (T_o) is an additional state variable which is estimated by the extended Kalman Filter.

5. Estimation algorithm

The discussed disturbance observer is based on the extended Kalman filter algorithm. Its flowchart is presented in Fig. 2. In general, EKF based estimation is realized in two steps: prediction and actualization. The estimated state vector is given by the following formula [2, 29, 31]:

$$\hat{\mathbf{x}}_{k|k} = \hat{\mathbf{x}}_{k|k-1} + \mathbf{K}_k [\mathbf{y}_k - \mathbf{C}\hat{\mathbf{x}}_{k|k-1}], \quad (23)$$

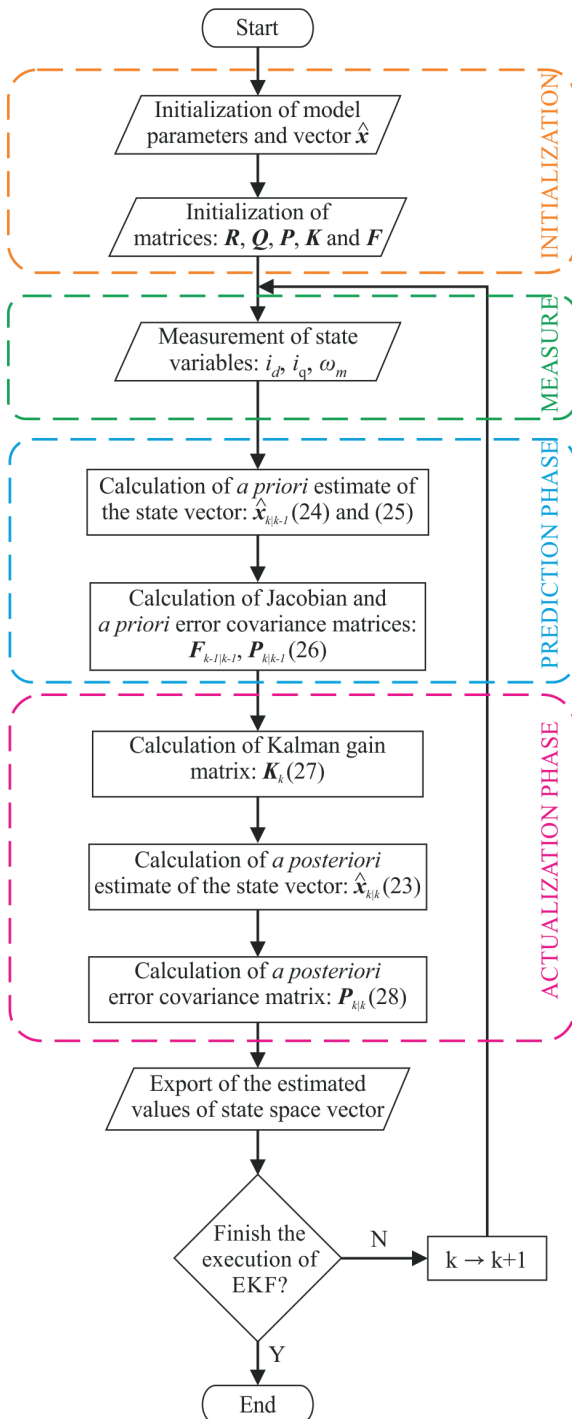


Fig. 2. Flowchart of the estimation algorithm based on EKF

where: $\hat{\mathbf{x}}_{k|k}$, $\hat{\mathbf{x}}_{k|k-1}$ – *a posteriori* and *a priori* estimate of the state vector, respectively, \mathbf{K}_k – Kalman gain matrix.

The *a priori* estimate is calculated in the prediction step and it is based on the defined mathematical model of the system (21), omitting the process noise, it may be rewritten in the following form [2, 28, 31]:

$$\hat{\mathbf{x}}_{k|k-1} = \mathbf{A}_{d_{k-1|k-1}} \hat{\mathbf{x}}_{k-1|k-1} + \mathbf{B}_d \mathbf{u}_{k-1}. \quad (24)$$

This formula is used to calculate the predicted value of state-space variables. Since the state matrix $\mathbf{A}_{d_{k-1|k-1}}$ is non-stationary, it is necessary to recalculate its values in each prediction step. The predicted value of overall disturbance was extended by introducing a correction term related to the integral of the tracking-error for estimated angular velocity. It is given by the following equation [31]:

$$\hat{\mathbf{T}}_{o_{k|k-1}} = \hat{\mathbf{T}}_{o_{k-1|k-1}} + L T_s [\omega_{m_k} - \hat{\omega}_{m_{k|k-1}}], \quad (25)$$

where: L – gain coefficient of the integral of tracking error. The introduced gain coefficient L was determined using a trial-and-error procedure to ensure the highest possible dynamic properties and maintaining a low impact of measurement noise on the control system simultaneously. The selected value was a compromise between the dynamics of the estimator and drive performance [31].

At this stage the *a priori* error covariance matrix should be also calculated. The equation can be defined as follows [28, 29, 31]:

$$\mathbf{P}_{k|k-1} = \mathbf{F}_{k-1|k-1} \mathbf{P}_{k-1|k-1} \mathbf{F}_{k-1|k-1}^T + \mathbf{Q} \quad (26)$$

with:

$$\mathbf{F}_{k-1|k-1} = \left. \frac{\partial \mathbf{f}(\mathbf{x}_k, \mathbf{u}_k, k)}{\partial \mathbf{x}_k} \right|_{\mathbf{x}_k = \hat{\mathbf{x}}_{k-1|k-1}} =$$

$$= \begin{bmatrix} 1 - \frac{T_s R_s}{L_s} & T_s p \omega_m & T_s p i_q & 0 \\ -T_s p \omega_m & 1 - \frac{T_s R_s}{L_s} & -T_s p \left(i_d + \frac{\Psi_f}{L_s} \right) & 0 \\ 0 & T_s \frac{K_t}{J_m} & 1 & -\frac{T_s}{J_m} \\ 0 & 0 & 0 & 1 \end{bmatrix}_{k-1|k-1},$$

where: $\mathbf{P}_{k|k-1}$ – *a priori* error covariance matrix, $\mathbf{F}_{k-1|k-1}$ – Jacobian matrix of the system, $\mathbf{P}_{k-1|k-1}$ – *a posteriori* error covariance matrix in the $k-1$ step, \mathbf{Q} – system covariance matrix. After calculating of *a priori* error covariance matrix, the estimation algorithm skips into actualization phase.

The actualization phase realizes the correction of the *a priori* estimated state-space vector based on equation (23). The correction corresponds to the output error between measured signals and estimated state variables. In such a case, it is necessary to calculate the Kalman gain matrix, which is given by the following equation [28, 29, 31]:

$$\mathbf{K}_k = \mathbf{P}_{k|k-1} \mathbf{H}_{k|k-1}^T \left[\mathbf{H}_{k|k-1} \mathbf{P}_{k|k-1} \mathbf{H}_{k|k-1}^T + \mathbf{R} \right]^{-1} \quad (27)$$

with:

$$\mathbf{H}_{k|k-1} = \left. \frac{\partial \mathbf{h}(\mathbf{x}_k, k)}{\partial \mathbf{x}_k} \right|_{\mathbf{x}_k = \hat{\mathbf{x}}_{k|k-1}} = \begin{bmatrix} 1 & 0 & 0 & 0 \\ 0 & 1 & 0 & 0 \\ 0 & 0 & 1 & 0 \end{bmatrix},$$

where: $\mathbf{H}_{k|k-1}$ – Jacobian matrix of the output, \mathbf{R} – output covariance matrix. It should be noted that since the system output is given as a linear function, the Jacobian matrix of the system output is constant and state independent.

The Kalman gain matrix is calculated for each actualization phase, after that the correction of estimated *a priori* state vector occurs. The *a posteriori* values of estimated state variables are obtained in regard to equation (23). The last operation of actualization phase is the calculation of *a posteriori* error covariance matrix, which is given by [28, 29, 31]:

$$\mathbf{P}_{k|k} = [\mathbf{I} - \mathbf{K}_k \mathbf{H}_{k|k-1}] \mathbf{P}_{k|k-1}, \quad (28)$$

where: $\mathbf{P}_{k|k}$ – *a posteriori* error covariance matrix, \mathbf{I} – unit matrix.

The chosen covariance matrices \mathbf{Q} and \mathbf{R} were obtained using a trial-and-error procedure. The matrices have a following form:

$$\mathbf{Q} = \text{diag} \left(\begin{bmatrix} 1.0 & 2.0 & 1.5 & 0.1 \end{bmatrix} \right), \quad (29)$$

$$\mathbf{R} = \text{diag} \left(\begin{bmatrix} 10.0 & 10.0 & 150.0 \end{bmatrix} \right). \quad (30)$$

The selected matrices ensure a proper operation of the disturbance observer and a sufficient dynamics of estimation. The depicted values were chosen to ensure the estimation ability of the periodic disturbance component. Values of system covariance matrix \mathbf{R} determine the behavior of estimated state variables. For a relatively small value the estimated signal entrusts more to the measurements, whereas for higher values the estimated variables follow the assumed mathematical model more. Too small or too large values cause unstable EKF operation, in such a case the estimated disturbance signal becomes oscillating. In this particular case the values in the range of $\langle 1; 190 \rangle$ ensure proper operation of the estimator without oscillations. The performed analysis indicates that for proper estimation of periodic disturbance in a PMSM drive, the values of the coefficients of the system covariance matrix \mathbf{R} should be possibly small for the current components i_d and i_q , whereas for the angular velocity should be possibly high.

6. Controller structure

The considered control system is based on a state feedback controller enhanced by a feedforward path, employed for compensation of the periodic disturbances [2, 31]. The estimated disturbance signal is introduced to the control loop through the feedforward, which allows to reduce the angular velocity ripple caused by the pulsating torque. The synthesis of a SFC requires a mathematical model of the plant given in state-space

representation [2, 31]. Rewriting equations (10)–(12), a following continuous model is obtained [2]:

$$\frac{d\mathbf{x}(t)}{dt} = \mathbf{A}(\omega_m)\mathbf{x}(t) + \mathbf{B}\mathbf{u}(t) + \mathbf{E}d(t) \quad (31)$$

with:

$$\mathbf{A}(\omega_m) = \begin{bmatrix} -\frac{R_s}{L_s} & p\omega_m(t) & 0 \\ -p\omega_m(t) & -\frac{R_s}{L_s} & -p\frac{\Psi_f}{L_s} \\ 0 & \frac{K_t}{J_m} & 0 \end{bmatrix},$$

$$\mathbf{x}(t) = \begin{bmatrix} i_d(t) \\ i_q(t) \\ \omega_m(t) \end{bmatrix}, \quad \mathbf{B} = \begin{bmatrix} \frac{K_{pp}}{L_s} & 0 \\ 0 & \frac{K_{pp}}{L_s} \\ 0 & 0 \end{bmatrix}, \quad \mathbf{E} = \begin{bmatrix} 0 \\ 0 \\ -\frac{1}{J_m} \end{bmatrix},$$

$$\mathbf{u}(t) = \begin{bmatrix} u_{sd}(t) & u_{sq}(t) \end{bmatrix}^T, \quad d(t) = T_o(t),$$

where: $\mathbf{A}(\omega_m)$ – non-stationary state matrix (continuous-time domain), \mathbf{B} – input matrix, $\mathbf{x}(t)$ – state vector, \mathbf{E} – disturbance matrix, $\mathbf{u}(t)$ – input vector of normalized voltage signals $u_{sd}(t)$ and $u_{sq}(t)$, $d(t)$ – disturbance, K_{pp} – the value of inverter gain. It should be noted that the dependence between the input voltages given in (10) and (11) and the above mentioned normalized signals is as follows:

$$\begin{bmatrix} u_d(t) \\ u_q(t) \end{bmatrix} = K_{pp} \begin{bmatrix} u_{sd}(t) \\ u_{sq}(t) \end{bmatrix}. \quad (32)$$

Since the above mentioned model contains cross-coupling of state variables it is non-stationary. In such a case, the application of a stationary controller requires a linear plant, therefore a simple linearization method has been employed. It assumes the introduction of additional non-linear control signals into the system, described by following equations [2, 31]:

$$u_{dd}(t) = -\frac{pL_s\omega_m(t)i_q(t)}{K_{pp}}, \quad (33)$$

$$u_{qd}(t) = \frac{p\omega_m(t) [L_s i_d(t) + \Psi_f]}{K_{pp}}, \quad (34)$$

where: $u_{dd}(t)$, $u_{qd}(t)$ – decoupling signals introduced into system for d and q axis, respectively.

In terms of operation under non-zero disturbance and load torque conditions, to obtain zero steady-state error for step changes of the reference value of angular velocity $\omega_{m\text{ref}}$ and load torque T_l , two additional state-variables were introduced into the control system. They correspond to the internal model

of the reference signal given by [2, 31]:

$$p_{i_d}(t) = \int_0^T [i_d(\tau) - i_{d\text{ref}}(\tau)] d\tau, \quad (35)$$

$$p_{\omega_m}(t) = \int_0^T [\omega_m(\tau) - \omega_{m\text{ref}}(\tau)] d\tau, \quad (36)$$

where: $p_{i_d}(t)$, $p_{\omega_m}(t)$ – introduced state variables corresponding to integrals of the error of d -axis current component $i_d(\tau)$ and angular velocity $\omega_m(\tau)$, respectively, $i_{d\text{ref}}(\tau)$, $\omega_{m\text{ref}}(\tau)$ – reference values of the d -axis current component and angular velocity, respectively.

Taking into account equations (33)–(36) in equation (31) and omitting the disturbance, a stationary extended state-space model is obtained [2]:

$$\frac{d\mathbf{x}_e(t)}{dt} = \mathbf{A}_e \mathbf{x}_e(t) + \mathbf{B}_e \mathbf{u}_e(t) + \mathbf{F} \mathbf{r}(t) \quad (37)$$

with:

$$\mathbf{x}_e(t) = \begin{bmatrix} i_d(t) \\ i_q(t) \\ \omega_m(t) \\ p_{i_d}(t) \\ p_{\omega_m}(t) \end{bmatrix}, \quad \mathbf{A}_e = \begin{bmatrix} -\frac{R_s}{L_s} & 0 & 0 & 0 & 0 \\ 0 & -\frac{R_s}{L_s} & 0 & 0 & 0 \\ 0 & \frac{K_t}{J_m} & 0 & 0 & 0 \\ 1 & 0 & 0 & 0 & 0 \\ 0 & 0 & 1 & 0 & 0 \end{bmatrix},$$

$$\mathbf{u}_e(t) = \begin{bmatrix} u_{dl}(t) \\ u_{ql}(t) \end{bmatrix}, \quad \mathbf{B}_e = \begin{bmatrix} \frac{K_{pp}}{L_s} & 0 & 0 & 0 & 0 \\ 0 & \frac{K_{pp}}{L_s} & 0 & 0 & 0 \end{bmatrix}^T,$$

$$\mathbf{r}(t) = \begin{bmatrix} i_{d\text{ref}}(t) \\ \omega_{m\text{ref}}(t) \end{bmatrix}, \quad \mathbf{F} = \begin{bmatrix} 0 & 0 & 0 & -1 & 0 \\ 0 & 0 & 0 & 0 & -1 \end{bmatrix}^T,$$

where: \mathbf{A}_e , \mathbf{B}_e , \mathbf{F} – extended state, input and reference matrices of the system, $\mathbf{x}_e(t)$ – enhanced state vector, $\mathbf{u}_e(t)$ – linearized input vector ($u_{dl}(t) = u_{sd}(t) - u_{dd}(t)$, $u_{ql}(t) = u_{sq}(t) - u_{qd}(t)$), $\mathbf{r}(t)$ – vector of reference signals.

Based on the model of the plant presented before, a following control law may be defined [2]:

$$\mathbf{u}_e(t) = -\mathbf{K}_x \mathbf{x}_e(t) - \mathbf{K}_{ff} \hat{T}_o(t), \quad (38)$$

where: \mathbf{K}_x , \mathbf{K}_{ff} – introduced control gain and feedforward matrices. The first matrix corresponds to the given state-variables, whereas the second one is introduced for compensation of disturbances present in the drive system. The block diagram of proposed control structure is shown in Fig. 3.

In order to ensure safe operation of the drive, a model predictive approach constraint (MPAC) method was employed for limitation of the quadrature current $i_q(t)$. Detailed information

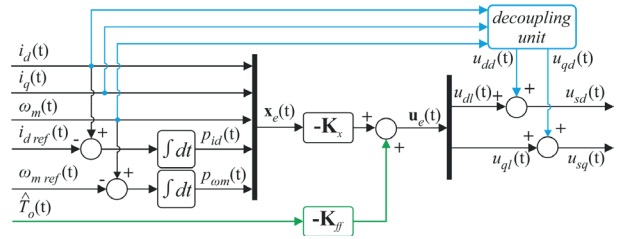


Fig. 3. Block diagram of employed controller structure

about the above mentioned constraint handling method can be found in [2, 18, 31].

Implementation of the designed control structure into a microcontroller based system requires a redefinition of the continuous control law (38) into a discrete form. In such a case, the integral operation may be replaced by its discrete counterpart – backward Euler method. It should be noted that proper operation of the control system needs linear operation of the modulator, therefore the allowed values of control signals should be limited to ± 1 . In order to limit the negative impact of the windup phenomenon additional anti-windup path has been introduced into the control system. Taking the above into account, the equation (36) shall be rewritten in the discrete form as follows:

$$p_{\omega_{m_k}} = p_{\omega_{m_{k-1}}} + T_s [e_{\omega_{m_k}} - k_{awu} u_{q_{awu_{k-1}}}], \quad (39)$$

where: $p_{\omega_{m_k}}$ – value of the velocity integral in k^{th} sampling period, $e_{\omega_{m_k}}$ – difference between the value of angular velocity ω_{m_k} and the given reference value $\omega_{m\text{ref}}$ in k^{th} sampling period, k_{awu} – anti-windup gain coefficient, $u_{q_{awu_{k-1}}}$ – the value of control signal overflow in $k^{\text{th}} - 1$ sampling period.

The controller gain coefficients were obtained using a discrete *linear-quadratic* optimization method provided in the Mathworks Matlab software (*lqrd*). The control matrix has the following form:

$$\mathbf{K}_x = \begin{bmatrix} 0.22 & 8.14 & 0.0 & 0.0 & 0.0 \\ 0.0 & 0.0 & 0.08 & 0.06 & 4.05 \end{bmatrix}. \quad (40)$$

The feedforward matrix was calculated using a method based on residual model of the plant, given by the following equation [31]:

$$\mathbf{K}_{ff} = [\mathbf{K}_x \quad \mathbf{I}] [\mathbf{A}_{e_{3 \times 3}} \quad \mathbf{B}]^{-1} \mathbf{E} = \begin{bmatrix} 0 & 0.078 \end{bmatrix}^T, \quad (41)$$

where: \mathbf{I} – unit matrix, $\mathbf{A}_{e_{3 \times 3}}$ – submatrix equal to first three rows and columns of the matrix \mathbf{A}_e .

7. Experimental results

The designed disturbance estimator and control structure were implemented in a prototype drive (Fig. 5A) with PMSM (Fig. 5B). The laboratory setup (Fig. 5) is equipped in a main drive unit consisting of: PMSM (LTi Drives LST-127-2-30-560)

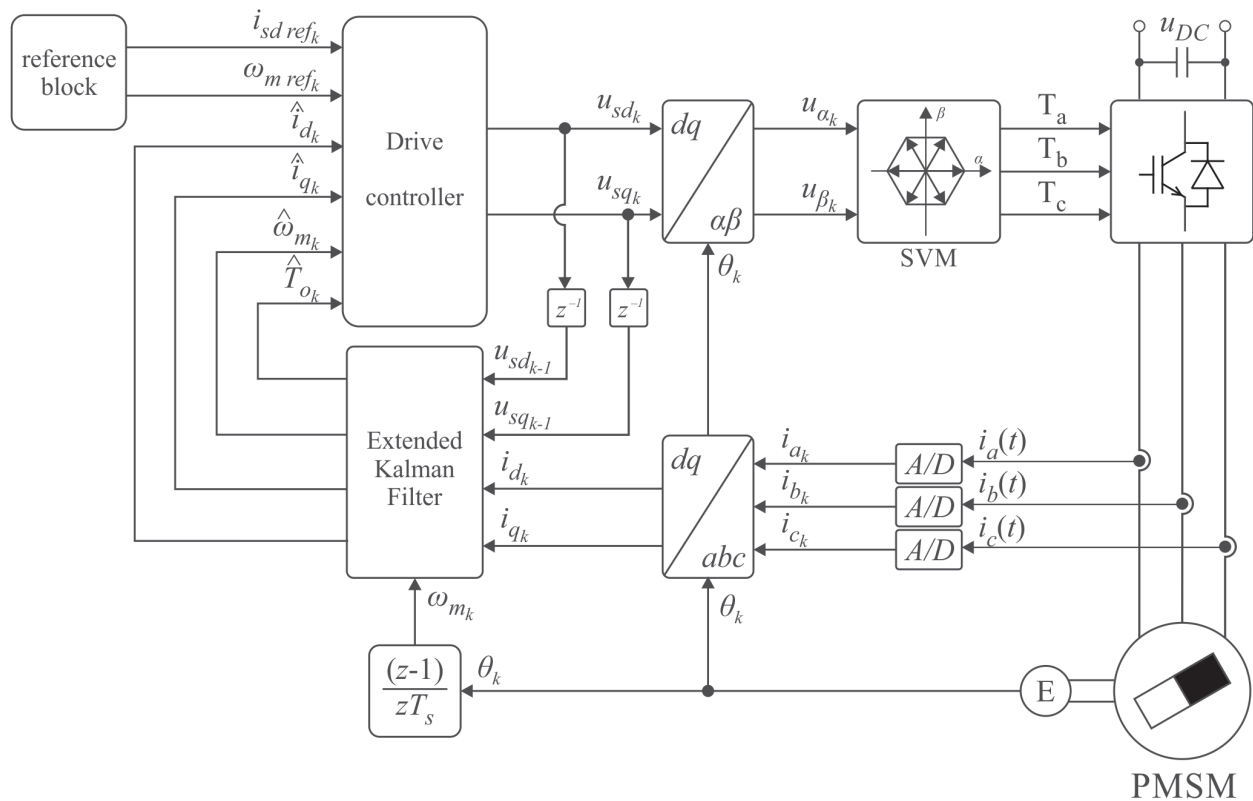


Fig. 4. Block diagram of the drive system with disturbance estimator based on extended Kalman filter algorithm

fed by a prototype 2-level VSI with IGBT power semiconductor devices based on ARM Cortex-M4 core (STMicroelectronic STM32F407VGT6), and a load drive unit with PMSM. The main parameters of the investigated drive system are summarized in Table 1.

Table 1
The main parameters of investigated drive system

Parameter	Symbol	Value	Unit
Input power	P_N	1000	W
Input current	I_{DC}	5.0	A_{rms}
Rated speed	N_n	1000	rpm
Rated torque	T_n	8.1	Nm
Stator resistance	R_s	1.05	Ω
Stator inductance	L_s	12.7	mH
Torque constant	K_t	1.14	Nm/A
Number of pole-pairs (poles)	$p (n_p)$	3 (6)	–
Number of stator slots	n_s	27	–
Total moment of inertia	J_m	8.8×10^{-3}	kgm^2
Switching frequency	f_{sw}	10.0	kHz
Sampling time	T_s	100	μs
Tracking error gain of EKF	L	-700	Nm/rad

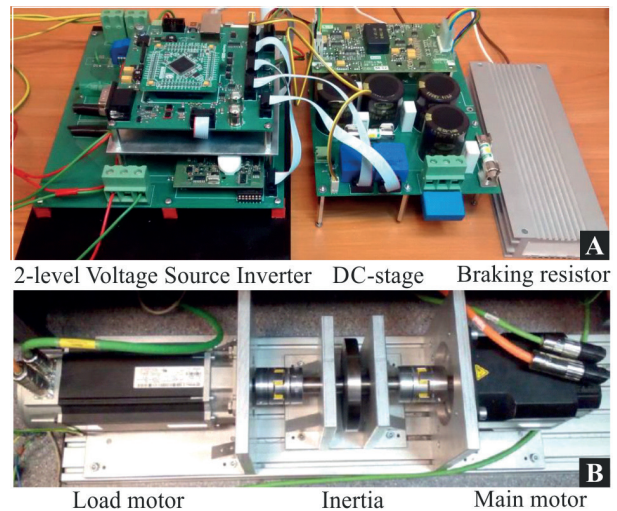


Fig. 5. Photo of laboratory setup: (A) Inverter unit, (B) mechanical unit

The experimental tests were carried out on the presented laboratory setup. The disturbance estimator based on extended Kalman filter algorithm was introduced into a drive control system for angular velocity regulation of the PMSM. The overall block diagram of considered control structure is presented on Fig. 4. The estimated state variables are introduced into control algorithm in order to ensure high performance of the drive system. A control strategy with zero direct current component was employed.

The experimental investigations were realized for several values of rotational speed of the drive in the low-speed operation area. The estimated disturbance signal was analyzed for a given speed set-point in steady-state for one mechanical revolution of the motor shaft. A detailed Fourier analysis of the estimated disturbance signal was carried out. For each investigated case, a frequency spectrum was determined. The obtained frequency-domain was investigated in the particular emphasis for the presence of specific harmonics in the spectrum defined by equations (7)–(9). A well-designed disturbance estimator has to be able to calculate properly of the estimated signals. In such a case the observed overall load should contain all the disturbance components present in the drive system. The obtained results are presented in Fig. 6. Since the periodic disturbance affects mainly the angular velocity in low-speed region [1, 2, 5], the experimental tests were carried out for several rotational speeds of the motor: 10, 20, 30 and 50 rpm. The left column (Figs. 6A–D) consists of estimated load signal in time-domain for a single revolution of the motor shaft. The obtained analysis in frequency-domain is shown in the right column (Figs. 6E–H).

Analyzing the time-domain data some features can be recognized: the shape of estimated disturbance signals is similar for different rotational speeds, the estimated signals contain a constant component and for each revolution of the shaft three periods can be distinguished in the disturbance signal. The last feature indicates that the disturbance in steady-state is speed-independent and is related to the position of the motor shaft, while the constant component is caused by a combination of Stribeck's effect, viscous friction and Coulomb friction. The periodic nature of the estimated signal is caused by the construction of the motor, the investigated machine contains three pole-pairs and therefore the same amount of periods occurs in the estimated disturbance signal. The obtained results are in line with the expectations, which confirms initially the proper operation of the employed extended Kalman filter.

The frequency-domain analysis ensures additional information in the field of estimation quality of the considered system. The obtained harmonic content (Figs. 6E–H) includes several components for each estimated disturbance signal. The analysis was carried out for harmonics in the range from 1st to 60th. It should be noted that since the investigated motor contains three pole-pairs the basic component for the phase currents is three times higher than the set angular velocity of the drive. Therefore, current related components of the disturbance have to be recognized for 3-times higher orders of harmonics than its usually occurs. Investigating the harmonics present in the disturbance (Figs. 6E–H), it can be seen that in all cases the following components stand out: 1st, 3rd, 6th, 12th, 18th, 27th, 36th and 54th. The first of them is related to the mechanical system, which is caused by mechanical imperfections (i.e. shaft misalignments) resulting in varying friction during one revolution [1]. The other components are connected with phenomena mainly caused by the inverter, motor construction and manufacturing imperfections [1, 6, 10, 23]. The 3rd harmonic is from the phase currents point-of-view the first harmonic, which indicates that its presence is connected with the offset errors in measure-

ment paths of the stator currents, caused by the inverter [1, 6]. In case of the 6th harmonic component the issue is slightly different, but still, from the stator currents point-of-view it is the second order component. The difference is implicated by two separated sources, and therefore this specific harmonic is a sum of current scaling error of phase currents [6] and the first AHC of cogging effect (9) caused by manufacturing imperfections of the stator, related to the number of poles n_p [23, 25]. The AHC introduces also the 12th harmonic component of the disturbance (every sixth). The next group of harmonics, i.e. 18th and 36th, is related to several components of pulsating torque present in PM AC drives. Since the investigated drive has three pole-pairs, the aforementioned harmonics related to the fundamental of phase currents is the 6th and 12th component, recognized as dead-time effect, flux variations and AHC of cogging torque (7)–(9) [1, 6, 23, 25]. The presence of cogging effect introduces into drive system a disturbance called additional harmonic content, which is related to the material and manufacturing imperfections, i.e. mounting misalignment, permanent magnets and stator teeth misplacement [23, 25, 27]. The last group of harmonics, i.e. 27th and 54th is related to both AHC and NHC of cogging torque, caused by stator construction and manufacturing accuracy. Since the investigated motor contains 27 stator slots the least common multiple of number of poles and slots ($\text{LCM}(n_s, n_p)$) is equal 54, which gives, in respect to equation (9), the first order of NHC [23, 27]. The manufacturing imperfections caused by mounting misplacement of PMs introduces the AHC related to the number of stator slots n_s , which is recognized as the 27th harmonic present in the frequency domain.

The above analysis indicates that the proposed estimator algorithm can be successfully implemented into a microcontroller based drive system and is able to estimate all expected components of periodic disturbance present in a drive system with PMSM.

The developed disturbance estimator was employed for ripple reduction of angular velocity. The effectiveness of disturbance compensation was investigated in respect to selected operation range of the drive, i.e. 10–50 rpm. The aim of this stage of experimental tests was to determine the rejection ability of pulsating torque using the proposed control structure. The angular velocity of the motor was analyzed in steady-state for two variants, the first of them was carried out with an open feedforward loop (*compensation off*), whereas in the second case the feedforward was closed (*compensation on*). Each of the variants was employed for a time interval equal to the half of the experiment duration. The results are presented in Fig. 7 in time- (Figs. 7A–D) and frequency-domain (Figs. 7E–H). The time-domain data indicates that a significant reduction of velocity ripple is achieved using the proposed control system. The obtained results indicate that the proposed disturbance estimator based on EKF algorithm may be successfully employed for reconstruction of pulsating torque in a drive with PMSM. The harmonic content of the frequency-domain for the angular velocity corresponds to the results obtained for estimated disturbance. All of the components, caused by the discussed phenomena (7)–(9),

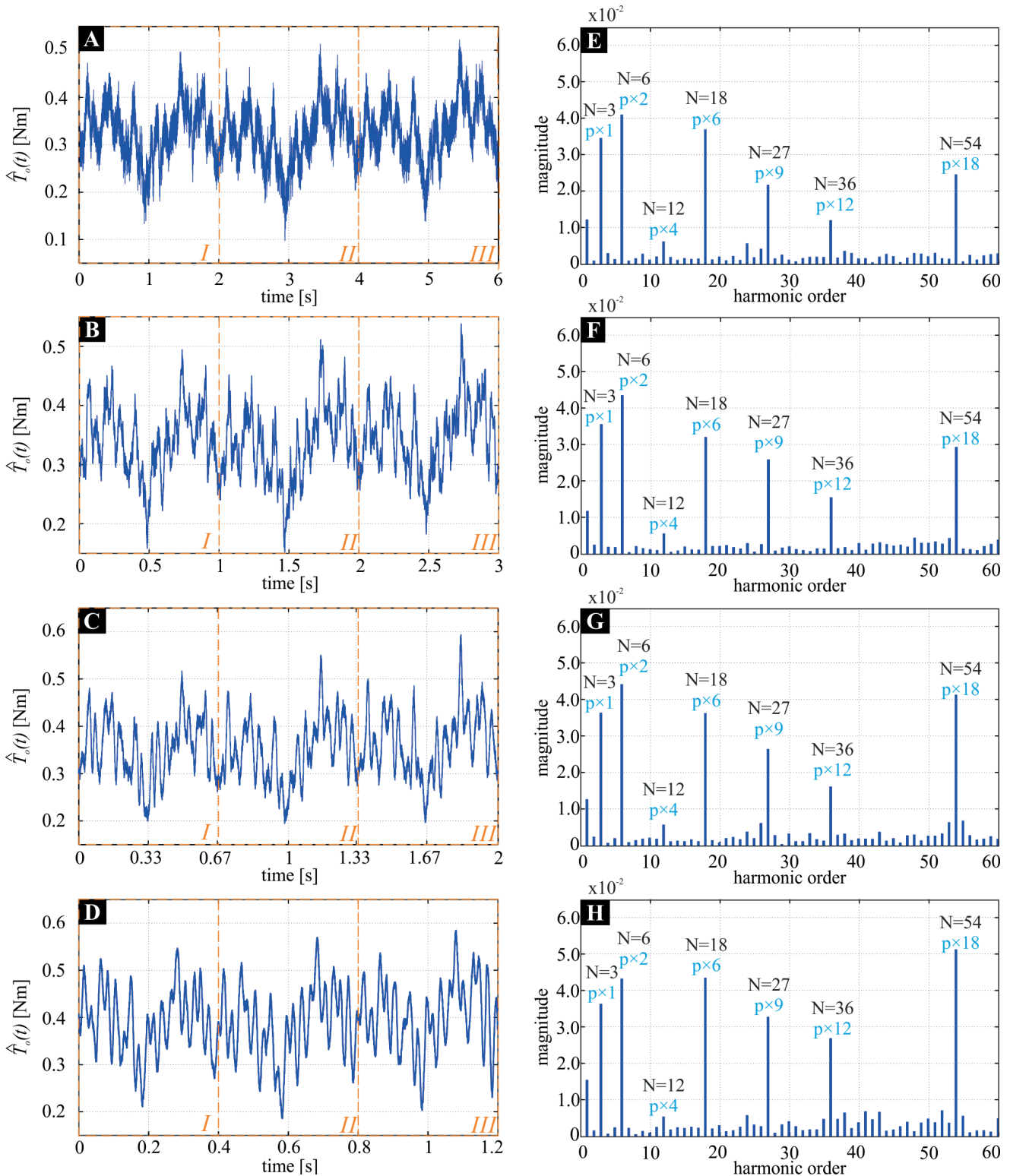


Fig. 6. Experimental results – estimated disturbance: overall load (left column), harmonics content of estimated disturbance (right column) for rotational speed of: 10 (A), 20 (B), 30 (C) and 50 (D) rpm

are highly attenuated. In such a case it should be noted that the experimental results indicate the following: 1) extended Kalman filter may be successfully employed for estimation of periodic disturbances present in drive systems with PMSM,

2) the design process of EKF is not a trivial task, and therefore it is highly time consuming, 3) the introduction of proposed control system enhances the operation quality of the drive.

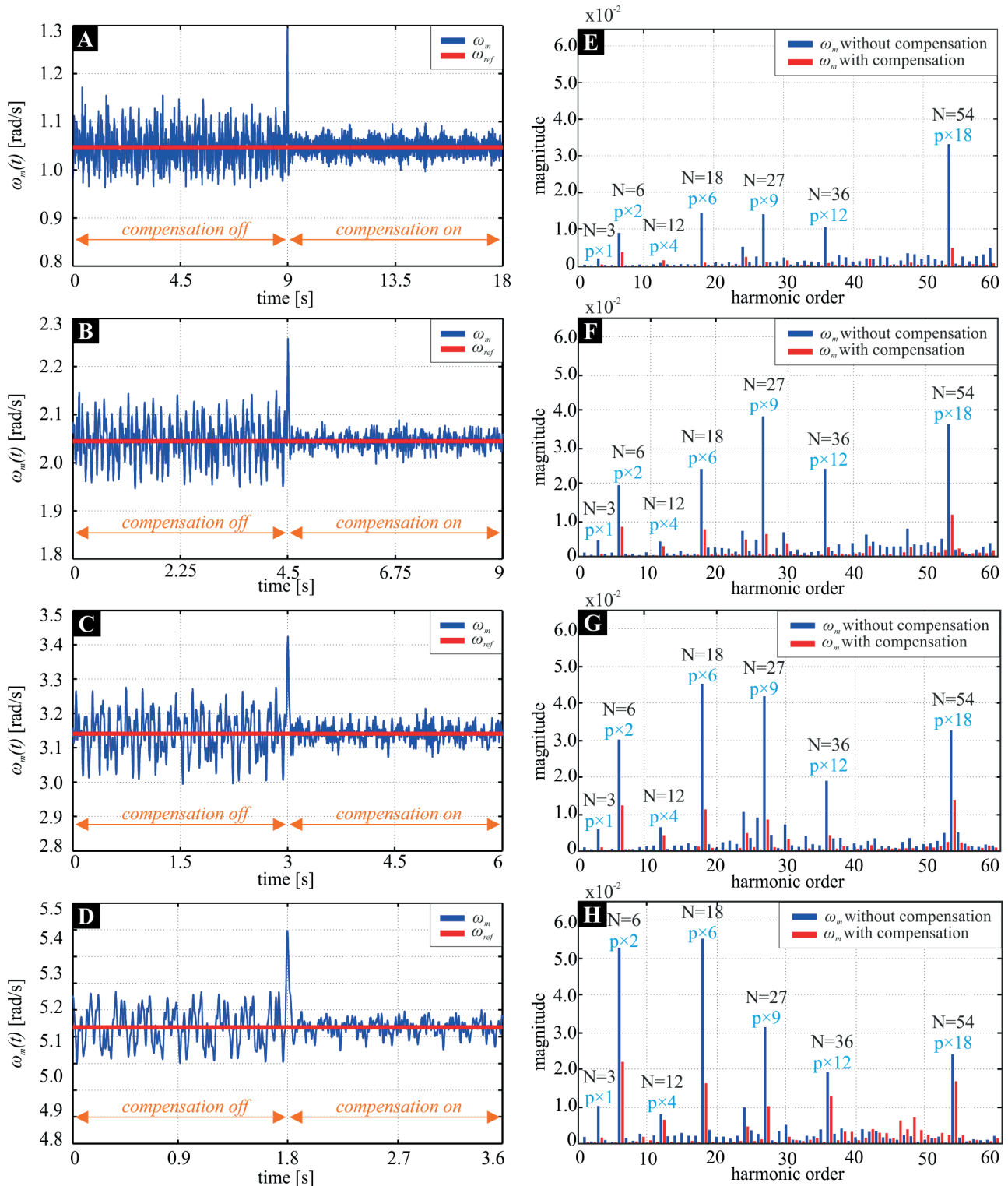


Fig. 7. Experimental results for introduced compensation method of periodic disturbance: angular velocity (left column), harmonics content (right column) for rotational speeds of: 10 (A), 20 (B), 30 (C) and 50 (D) rpm.

8. Conclusions

In this paper disturbance estimation and attenuation abilities of EKF based observer in a PMSM drive were investigated. Extended Kalman filter algorithm was adopted and implemented

into a drive system with PMSM. The designed state-vector observer was employed for estimation of overall load torque containing the periodic disturbance component. That is achieved by introducing a full order mathematical model of the drive given in dq -frame. The estimated disturbance contains all expected

harmonics, which confirms indirectly the proper operation of the designed EKF.

The experimental tests were carried out for several rotational speeds of the motor in low-speed operating range, i.e. 1–5% of rated speed. The analysis of EKF estimation was conducted for steady-state at given rotational speed of the drive. The obtained results were presented in time- and frequency-domain for a single revolution of the motor shaft. At first it was concluded that the obtained signals are periodic and contain three periods for each revolution of the motor shaft, which was in the line with the expectations, since the investigated PMSM had three pole-pairs. Subsequently, a frequency-domain analysis was carried out. Discrete Fourier transform was calculated for the given fundamental, equal to the angular velocity of the drive. The results of the analysis indicate that the estimated disturbance signal contains all of the expected components for each of investigated operating points. The obtained frequency spectra contain components related to: shaft misalignments ($N = 1$), phase currents measurement errors ($N = 3$ and $N = 6$), torque ripple components, i.e. dead time effect and mutual torque ($N = 18$ and $N = 36$), and cogging effect: $AHC\{n_P, n_S\}$ ($N = 6$, $N = 12$, $N = 18$, $N = 27$, and $N = 54$) and NHC ($N = 54$). Some of the identified phenomena overlap, and therefore it is impossible to determine the impact of particular sources on the magnitude of the produced harmonic. This inconvenience is not a problem in general, because the first goal of the research was to design a disturbance observer able to estimate properly all periodic components present in the drive system. Whereas, the final goal of the performed tests was to employ the disturbance observer for disturbance attenuation. The obtained results indicate that the estimated pulsating torque may be introduced into the control system for enhancement of operation quality of the drive. In order to realize compensation of periodic disturbances, a feedforward path shall be introduced into a state feedback controller. The proposed control structure significantly reduces the value of angular velocity ripple. The attenuation of periodic disturbances is successfully realized using a SFC with feedforward and EKF.

Acknowledgements. This research was supported by the basic research fund of the Department of Automatics and Measurement Systems, Nicolaus Copernicus University, Poland.

REFERENCES

- [1] J. Yang, W. Chen, S. Li, L. Guo, and Y. Yan, “Disturbance/Uncertainty Estimation and Attenuation Techniques in PMSM Drives – A Survey”, *IEEE Trans. on Ind. Electron.* 64 (4), 3273–3285 (2017).
- [2] Ł.J. Niewiara, T. Tarczewski, and L.M. Grzesiak, “Application of State Feedback Controller with Feedforward for velocity ripples reduction of PMSM drive at low speed operation”, *21st Eur. Conf. on Power Electron. and Appl. (EPE'19 ECCE Europe)*, Genova, 2019, pp. 1–10.
- [3] Y.A.-R.I. Mohamed and E. El-Saadany, “A current control scheme with an adaptive internal model for torque ripple minimization and robust current regulation in PMSM drive systems”, *IEEE Trans. Energy Convers.* 23 (1), 92–100 (2008).
- [4] S. Geng, Y. Zhang, H. Qiu, C. Yang, and R. Yi, “Influence of harmonic voltage coupling on torque ripple of permanent magnet synchronous motor”, *Arch. Elect. Eng.* 68 (2), 399–410 (2019).
- [5] K. Erwinski, K. Kowalski, and M. Paprocki, “Neural Network Contour Error Prediction of a Bi-axial Linear Motor Positioning System”, *16th Int. Conf. on Inform. in Control, Automat. and Robot. (ICINCO)*, 2019.
- [6] D.-W. Chung and S.-K. Sul, “Analysis and compensation of current measurement error in vector-controlled AC motor drives”, *IEEE Trans. on Ind. Appl.* 34 (2), 340–345 (1998).
- [7] R. Errouissi, M. Ouhrouche, W.-H. Chen, and A. Trzynadlowski, “Robust nonlinear predictive controller for permanent-magnet synchronous motors with an optimized cost function”, *IEEE Trans. Ind. Electron.* 59 (7), 2849–2858, (2012).
- [8] S. Chai, L. Wang, and E. Rogers, “A Cascade MPC Control Structure for a PMSM with Speed Ripple Minimization”, *IEEE Trans. Ind. Electron.* 60 (8), 2978–2987 (2013).
- [9] S. Li and H. Gu, “Fuzzy adaptive internal model control schemes for PMSM speed-regulation system”, *IEEE Trans. Ind. Informat.* 8 (4) 767–779 (2012).
- [10] B. Ferretti, G. Magnani, and P. Rocco, “Modeling, identification, and compensation of pulsating torque in permanent magnet AC motors”, *IEEE Trans. Ind. Electron.* 45 (6), 912–920 (1998).
- [11] A. Houari et al., “An Effective Compensation Technique for Speed Smoothness at Low-Speed Operation of PMSM Drives”, *IEEE Trans. Ind. Appl.* 54 (1), 647–655 (2018).
- [12] K. Urbanski, “A new sensorless speed control structure for PMSM using reference model”, *Bull. Pol. Ac.: Tech.* 65 (4), 489–496 (2017).
- [13] H. Liu and S. Li, “Speed control for pmsm servo system using predictive functional control and extended state observer”, *IEEE Trans. Ind. Electron.* 59 (2), 1171–1183 (2012).
- [14] S. Li, C. Xia, and X. Zhou, “Disturbance rejection control method for permanent magnet synchronous motor speed-regulation system”, *Mechatronics* 22 (6), 706–714 (2012).
- [15] T.M. Jahns and W.L. Soong, “Pulsating torque minimization techniques for permanent magnet AC motor drives—a review”, *IEEE Trans. on Ind. Electron.* 43 (2), 321–330 (1996).
- [16] E. Sariyildiz and K. Ohnishi, “Stability and robustness of disturbance observer-based motion control systems”, *IEEE Trans. Ind. Electron.* 62 (1), 414–422 (2015).
- [17] Y.-R. Mohamed, “A hybrid-type variable-structure instantaneous torque control with a robust adaptive torque observer for a high-performance direct-drive PMSM”, *IEEE Trans. Ind. Electron.*, 54 (5) 2491–2499 (2007).
- [18] T. Tarczewski, M. Skiwski, Ł.J. Niewiara, and L.M. Grzesiak, “High-performance PMSM servo-drive with constrained state feedback position controller”, *Bull. Pol. Ac.: Tech.* 66 (1), 49–58 (2018).
- [19] T. Pajchrowski, “Application of neural networks for compensation of torque ripple in high performance PMSM motor”, *19th Eur. Conf. on Power Electron. and Appl. (EPE'17 ECCE Europe)*, Warsaw, 2017, pp. 1–8.
- [20] T. Pajchrowski and A. Wojcik, “The problem of rotational speed unevenness in direct drives with permanent magnet synchronous motors”, *Przegląd Elektrotechniczny* 94 (5), 128–132 (2018).

- [21] T. Tarczewski, Ł. Niewiara, and L.M. Grzesiak, "Torque ripple minimization for PMSM using voltage matching circuit and neural network based adaptive state feedback control", *16th Eur. Conf. on Power Electron. and Appl.*, Lappeenranta, 2014, pp. 1–10.
- [22] Ł.J. Niewiara, T. Tarczewski, and L.M. Grzesiak, "Application of DC/DC/AC dual voltage source inverter for current harmonics reduction in PMSM drive", *19th Eur. Conf. on Power Electronics and Applications (EPE'17 ECCE Europe)*, Warsaw, 2017, pp. 1–9.
- [23] L. Gašparin and R. Fiser, "Impact of manufacturing imperfections on cogging torque level in PMSM", *IEEE 9th Int. Conf. on Power Electronics and Drive Systems*, Singapore, 2011, pp. 1055–1060.
- [24] S. Hwang and J. Kim, "Dead Time Compensation Method for Voltage-Fed PWM Inverter", *IEEE Trans. on Energy Convers.* 25 (1), 1–10 (2010).
- [25] J. Kim, M. Yoon, J. Hong, and S. Kim, "Analysis of cogging torque caused by manufacturing tolerances of surface-mounted permanent magnet synchronous motor for electric power steering", *IET Electric Power Appl.* 10 (8), 691–696 (2016).
- [26] Ł.J. Niewiara, T. Tarczewski, and L.M. Grzesiak, "Application of extended Kalman filter for estimation of periodic disturbance in PMSM drive", *Proceedings of the XIV Scientific Conference SENE'2019*, 2019, pp. 1–8.
- [27] Z.Q. Zhu, S. Ruangsinchaiwanich, and D. Howe, "Synthesis of cogging-torque waveform from analysis of a single stator slot", *IEEE Trans. on Ind. Appl.* 42 (3), 650–657 (2006).
- [28] D. Janiszewski, "Extended Kalman Filter Based Speed Sensorless PMSM Control with Load Reconstruction", *IECON 2006 32nd Ann. Conf. on IEEE Ind. Electron.*, Paris, 2006 pp. 1465–1468.
- [29] S. Bolognani, R. Oboe, and M. Zigliotto, "Sensorless full-digital PMSM drive with EKF estimation of speed and rotor position", *IEEE Trans. on Ind. Electron.* 46 (1), 184–191 (1999).
- [30] G.R. Gopinath and P.D. Shyama, "Sensorless control of PMSM using an adaptively tuned SCKF", *The Journal of Engineering* 2019 (17), 4304–4308 (2019).
- [31] Ł.J. Niewiara, "State feedback control for a PMSM drive with complex DC/DC/AC converter" (original title: Sterowanie ze sprzężeniem od wektora stanu napędu z silnikiem PMSM i przekształtnikiem złożonym DC/DC/AC), Ph.D. Thesis, Warsaw, Warsaw University of Technology, 2018.
- [32] L. Jarzebowicz, "Errors of a Linear Current Approximation in High-Speed PMSM Drives", *IEEE Trans. on Power Electron.* 32 (11), 8254–8257 (2017).
- [33] L. Jarzebowicz, "Impact of low switching-to-fundamental frequency ratio on predictive current control of PMSM: A simulation study", *25th International Workshop on Electric Drives: Optimization in Control of Electric Drives (IWED)*, 2018, pp. 1–5.